Surface switching statistics of rotating fluid: Disk-rim gap effects

Yuji Tasaka and Makoto Iima

Phys. Rev. E **95**, 043113 — Published 27 April 2017

DOI: 10.1103/PhysRevE.95.043113

Surface switching statistics of rotating fluid: disk-rim gap effects

Yuji Tasaka*
Laboratory for Flow Control, Hokkaido University, N13W8, Sapporo 060-8628, Japan

Makoto Iima
Graduate School of Science, Hiroshima University,
1-7-1 Kagamiyama, Higashi-hiroshima 739-8521, Japan
(Dated: April 5, 2017)

We examined the influence of internal noise on the irregular switching of the shape of the free surface of fluids in an open cylindrical vessel driven by a bottom disk rotating at constant speed [Suzuki, Iima, and Hayase, Phys. Fluids, **18**, 101701 (2006)]. A slight increase in the disk-rim gap (less than 3 % of the disk radius) was established experimentally to cause significant changes in this system, specifically, frequent appearance of the surface descending event connecting a nonaxisymmetric shape in strong mixing flow (turbulent flow) and an axisymmetric shape in laminar flow, as well as a shift in critical Reynolds number that define the characteristic states. The physical mechanism underlying the change is analyzed in terms of flow characteristics in the disk-rim gap, which acts as a noise source, and a mathematical model established from measurements of the surface height fluctuations with noise term.

PACS numbers: 47.32.-y, 47.20.-k, 47.27.Cn

I. INTRODUCTION

Fluid motion is governed by strongly non-linear dynamics, which means that slight changes in configuration can lead to significant changes in the motion, even in simple configurations. Rotating flows in a cylindrical vessel are categorized as among the simplest and most fundamental flow configurations in fluid mechanics. Despite the simplicity of the configuration, the fluid phenomena are quite complex. Instabilities created during spinning-up and spinning-down [1, 2] and vortex breakdowns [3] in closed configurations as well as instabilities in configurations with interfaces [4–7] are typical examples that challenge researchers in experimental, theoretical, and also numerical fields.

Recently, in rotating fluids in open cylindrical vessels driven by a bottom disk, rotating polygons on the free surface has been observed and analyzed [Fig. 1(a)] [8–16]. In the analysis, a shallow fluid layer and large free-surface deformations are considered. With increasing speed of rotation of the disk, various deformations of the free surface from ellipsoidal to hexagonal are observed. If the radius of the rotating bottom disk is much smaller than the radius of the inner lateral wall of the cylinder, other flow patterns such as periodic sloshing have been observed [8, 14].

With thicker fluid layers, complex temporal variations of the free surface, termed "surface switching", have been reported [17]. Surface switching involves the intermittent transition of the free surface shape from axisymmetric to nonaxisymmetric shapes, and vise versa, with cross sections that are almost all ellipsoidal. The transitions often occur with violent fluctuations in the free surface level. A typical sequence of surface switching involves [Fig. 1(b)]: (i) if the disk rotation is sufficiently fast, a descent of the axisymmetric free surface which then attaches to the bottom; (ii) & (iii) symmetry breaking of the free surface yielding nonaxisymmetric shapes; (iv) the detachment of the free surface from the bottom; and (v) with a nonaxisymmetric cross-section, the resulting free surface is subject to quasi-periodic oscillations and reverts to an axial-symmetrical shape, after which it again reattaches to the bottom as in (i).

During surface switching, the flow state is laminar if the surface shape is axisymmetric [Fig. 1(b)(i)] and turbulent (or fully disturbed) if it is nonaxisymmetric [18, 19]. Hence, surface descent is accompanied by a transition from turbulent to laminar flow and the significant surface descent and ascent constitute laminar-turbulent switching (LTS). The mechanism and dynamics of the surface ascending event, termed LTS (laminar → turbulent) [Fig. 1(b): (i)→(ii)→(iii))], were investigated in detail by Iima and Tasaka [20] in relation to resonance instability [13, 15, 20, 21].

The statistical aspects of LTS, surface descent with restoration of axial symmetry, termed LTS (turbulent → laminar), and critical Reynolds numbers, change significantly even under small changes in configuration (disk-rim gap). Actually, when using a well-controlled driving system generating less mechanical noise than that used in Suzuki *et al.* [17], a fixed rotation axis, and precise disk rotation control, we found that the rate of appearance of LTS events is significantly reduced [18, 19]. Furthermore, states involving surface switching are clearly distinguishable; featuring a flat rotation (FR) and a (quasi-)regular oscillation (RO) as nonaxisymmetric states, as well as LTS [19, 20]. Also, a hysteresis is clearly seen in the regime diagram, in contrast to the results found by Suzuki *et al.* [17] who reported no such behavior [19].

* tasaka@eng.hokudai.ac.jp

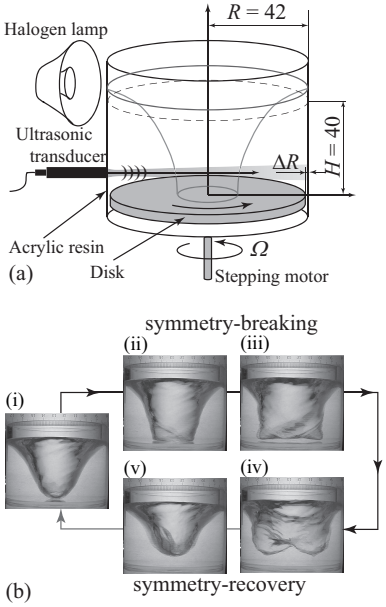

FIG. 1. (a) Experimental setup and measurement apparatus (unit mm). (b) Typical photographic sequence of surface switching showing surface shapes obtained with backlight projection.

In this paper, we focus on the influence of the disk-rim gap on the free surface motion and its statistical features, and in particular LTS appearances to illustrate free surface switching stemming from disk-rim gap details. Three disks of different diameter are chosen to change physically this gap with the objective of controlling the internal noise, namely, irregular fluctuations generated nearby the disk rim. Gap influences are investigated statistically, as well as dynamically, using radial velocity data and free-surface height fluctuations at the center of the cylinder. The physical mechanism underlying these changes is analyzed in regard to the noise generation from the disk-rim gap and its effect on surface switching dynamics, using a mathematical model that included effects from noise.

II. EXPERIMENTAL SETUP AND THE DISK-RIM GAP EFFECT

A. Experimental setup and procedures

In the experimental setup [Figure 1(a)], a disk is mounted at the bottom of an open, $R = 42$ mm radius cylindrical vessel made of acrylic resin. The disk is driven at constant rotation frequency, Ω, by a motor connected via a shaft. The vessel is partially filled with tap water to a height $H = 40$ mm at rest yielding an aspect ratio is $\mathcal{A} = H/R = 0.95$. There is a cavity with around 5 mm depth below the disk. We used ultrasonic velocity profiling (UVP) [19, 22, 23] to obtain details of the fluid flow, from which the velocity component of the instantaneous flow field along the direction of propagation of the ultrasonic waves is measured. An ultrasonic 4-MHz resonance frequency transducer is mounted on the lateral wall of the vessel; its center is 8 mm above the disk ($z/H = 0.2$). The line of propagation passes though the center of the vessel permitting radial component profiles of the instantaneous velocity field, $u_r(r,t)$, to be obtained. Ultrasonic reflecting particles, specifically 50–60 μm-diameter porous resin spheres of 1020 kg/m^3 density, were mixed into the test water. The spatial and temporal resolutions of the measurements depend on the set parameters; typical values are 0.74 mm and 13 ms, respectively. To capture the transitions in the surface shape, backlight projection images of the surface illuminated by a halogen lamp [cf. Fig. 1(b)] were recorded using a digital video camera at 29.97 frames per second. Time variations in the surface height along the centerline of the vessel, $h(t)$, were extracted from the video using simple image processing. Further details of the setup and measurements are given in Tasaka and Iima [19].

Based on the successful generation of local turbulence in flows between stationary and rotating disks [24], we used three different disks that gave three gap sizes between the inner lateral wall of the vessel and the rim of the disk, ΔR,. The three disks used here are (A) $\Delta R = 0.10$ mm (made of acrylic resin), (B) $\Delta R = 0.30$ mm (glass, also used in [19]), and (C) $\Delta R = 1.05$ mm (acrylic resin). All three disks are flat cylinders. The corresponding Reynolds number of the gap flow is defined as $\mathrm{Re}_g = 2\pi R\Omega\Delta R/\nu$. For $\Omega = 13.3$ Hz, a typical rotation frequency, $\mathrm{Re}_g = 0.35\times10^3$, 1.05×10^3, and 3.69×10^3, respectively, where ν is the kinematic viscosity of water. The characteristics of the three disks mentioned above are detailed in Table I for ease of reference.

With disks of different materials, glass and acrylic resin are thought to provide data regarding differences in wettability. We have previously suggested that the influence of wettability of the test fluid on the disk could be a reason for the increase in critical rotation speed for surface switching [19]. We have also previously confirmed that using glass disks with better wettability than the acrylic disk used in Tasaka *et al.* [18] results in increases in the frequency of LTS events leading to attachment of the free surface to the bottom [Fig. 1(b)]. Nevertheless, in most cases observed in the well-controlled system, the rotating free surface maintains a nonaxisymmetric shape above and away from the bottom surface [Fig. 1(b)–(iv)], and events where the surface touches the bottom do not occur very often. This would ensure that wettability does not affect LTS (turbulent $\rightarrow$ laminar) which is the focus of this report.

B. Significance of the disk-rim gap

Here we comment on why the disk-rim gap is important in the bottom-rotating setup. Assuming that the flow in the gap region is similar to Taylor–Couette flow

TABLE I. Specifications of disks

Disk	Gap size ΔR [mm]	Material	Expected internal noise level
(A)	0.10	Acrylic	low
(B)	0.30	Glass	moderate
(C)	1.05	Acrylic	high

(TCF) in concentric double cylinders [25], we may expect that noise increases with changes in disk from (A) to (C). With the inner cylinder rotating, usual TCF generates a modal shift with increasing Reynolds numbers at several flow regimes. The transition is from one that is time-periodic (wavy vortex flow) to one with turbulent Taylor vortices via intermediate regimes that have quasi-periodic flow and chaotic flow [cf. 26]. The evaluated Reynolds number of the gap flow, Re_g, mentioned in the last section, is a few thousand and the corresponding flow regime at TCF is chaotic or turbulent flow. The velocity fluctuations arising with the gap flow is highly complex, and noise is constantly generated in the bulk flow. Of the disks, disk (B) has been used in a previous study [19] and our comparative analysis starts with results obtained for this disk providing a basic reference of the phenomena.

III. RATE OF A SURFACE DECENT EVENT

All disks examined for this study showed surface switching [Fig. 1(b)] if the rotation frequency of the disk, Ω, surpasses the critical value of around 13 Hz. The corresponding Reynolds number of the rotating boundary layer on the disk, $\mathrm{Re} = 2\pi\Omega R^2/\nu$, takes values of order $O(10^5)$ setting the boundary layer turbulence at least near the disk edge according to the results of three-dimensional boundary layer on a rotating disk summarized in Reed and Saric [27]. We recorded the variation in the surface height at the center of the vessel, $h(t)$, for each disk: disk (A) (Ω = 13.3 Hz, $\mathrm{Re} = 1.47 \times 10^5$), disk (B) ($\Omega$ = 13.2 Hz, $\mathrm{Re} = 1.46 \times 10^5$), and disk (C) ($\Omega$ = 13.3 Hz, $\mathrm{Re} = 1.47 \times 10^5$). Figure 2 shows plots of the surface height fluctuations after removal of the fast oscillation using moving averages (see caption); these moving-averaged fluctuations are denoted $\langle h(t)\rangle$. The plots for panels (a)–(c) correspond to disks (A)–(C), respectively.

First, the characteristics of the fluctuations [Fig. 2(b)] for disk (B) are described as a basic reference for LTS events and characteristic quasi-stable states. The LTS events shown are distinguished by descents of the free surface approaching the bottom followed by ascents from the bottom position. There are two LTS events occurring during the 350-s video clip at around 170 and 330 s, the first being accompanied by the attachment of the free surface to the bottom disk.

Three characteristic states are observed. In the first state, the surface height fluctuations frequently assume quasi-regular oscillations (RO), which are maintained for some period (indicated as "RO"), and the free surface in this state displays clear humps [Fig. 2(b)(iv)] [19]. The center of the oscillation is located around $\langle h\rangle/H = 0.25$ and the amplitude is slightly modulated, not with a simple amplitude-modulated sinusoidal shape but with cusps at local maxima.

The second state is flat rotation (FR), where the free surface displays no significant humps [19]. This state is also maintained for some duration at around $t \sim 40$ and 250 s and the fluctuations have relatively small amplitudes (indicated as "FR"). The average location of the free surface in this state is around $\langle h\rangle/H = 0.31$ and is slightly higher than the central location of $\langle h\rangle/H$ in RO.

We also define a third "temporary axisymmetric (TA)" state observed at LTS events; this is an unstable state where the descending free surface almost recovers the axi-symmetry that leads to the resonance instability [13, 15, 20, 21]. Overall, the fluctuations appear to display switching in all the three states: RO, FR, and TA accompanying the LTS events. The flow structures in these states and the dynamics during the LTS are discussed in detail in Iima and Tasaka [20].

The slight changes in size of the disk-rim-gap cause very considerable changes in the permanence of the states appearing. In Fig. 2(a), with the smallest gap (disk (A)) for which we would expect the generation of less internal noise, the fluctuation shows the presence of the FR state over a large portion of the time series of $\langle h\rangle$, which is different in Fig. 2(b) with the larger gap (disk (B)). The fluctuations in Fig. 2(a) assume a central value around $\langle h\rangle/H = 0.31$, very similar to that for Fig. 2(b). Two LTS events occur in the measurement period and this number of occurrences is the same as with disk (B) [Fig. 2(b)]. However, different from disk (B), RO occurs less frequently and the amplitude of the oscillations is strongly modulated. Also the FR and RO states are not clearly separated (distinguishable) and the transitions between these two states are not clear.

In Fig. 2(c), for disk (C) with the largest gap, LTS events occur more frequently than with the other disks with narrower gaps. No FR is observed and the amplitude of the RO fluctuations is more strongly modulated. These observations are similar to surface switching phenomena reported by Suzuki *et al.* [17]. The differences in the surface height fluctuations for these three disks clearly suggest that the increase in noise generated in the disk-rim gap increases the frequency of LTS events and blurs the transition between different states. All three gap widths show a central height of the surface fluctuation at $h/H \sim 0.3$ suggesting that modifying the gap size does not cause qualitative changes in the flow structure at least for the range of gaps examined here.

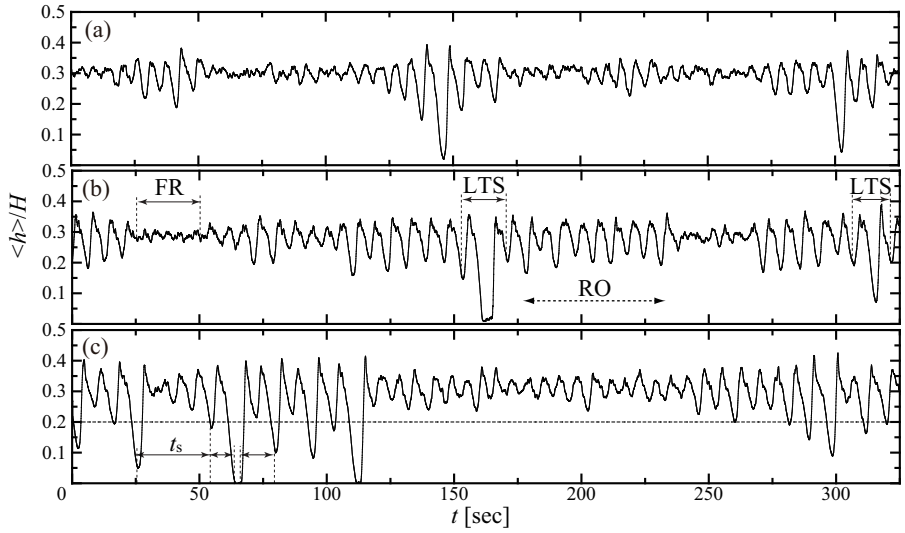

FIG. 2. Time series of the averaged surface height $\langle h \rangle$ for different disks, (a) disk (A) ($\Omega = 13.3$ Hz, Re $= 1.47 \times 10^5$), (b) disk(B) ($\Omega = 13.2$ Hz, Re $= 1.46 \times 10^5$), and (c) disk (C) ($\Omega = 13.3$ Hz, Re $= 1.47 \times 10^5$). The averaged surface height $\langle h \rangle$ is a moving average of the original surface-height data for the period corresponding to around seven rotations of the disk to remove the rapid fluctuations caused mainly by the rotating humps on the ellipsoidal free surface shown in Fig. 1(b)(iv). The solid arrows in (b) indicate periods including FR and LTS highlighted in Fig. 5(b). The dashed arrow in (b) indicates an example of the RO state in the time series. The arrows in (c) mark the time intervals of LTS events, t_s (dips extending below the broken line).

IV. FLOW REGIME AND HIGH INTENSITY BRANCH

A. Flow regimes shown by the intensity of flow fluctuations

Figure 3(a) shows the intensity of the temporal velocity fluctuations, V, plotted vs Re: V is defined as $V = 1/(2\pi\Omega(\eta_2 - \eta_1)R^2) \int_{\eta_1 R}^{\eta_2 R} u_{sp}(r)dr$ ($\eta_1 = 0.49$, $\eta_2 = 0.67$), $u_{sp} = [(1/T)\int_0^T u_r'(r,t)^2 dt]^{1/2}$ (where $u_r'(r,t)$ is the temporal fluctuation component of $u_r(r,t)$ and T is the measurement time). The recording time of the spatio-temporal velocity distribution is approximately 60 s and a 10-min relaxation time was instigated before taking measurements after changing the Re; this relaxation time is $O(10^6)$ times that of the disk rotation period and is 100 times the vertical oscillation period of the free surface in the RO states. The measurements for the different ΔR disks are distinguished by circles, triangles, and squares; open and solid symbols indicate values measured during the increasing and decreasing stages of Re, respectively.

For all disks used in the experiments, the intensity, V, increased abruptly at a critical value, Re $=$ Re$_c$, where the regime transition of the surface shape from an axisymmetric [Fig. 3(b)] to a nonaxisymmetric [Fig. 3(c)] shape is observed. Once the free surface assumes a nonaxisymmetric shape, it is maintained even when Re $<$ Re$_c$ in the decreasing Re stage until Re reaches a different critical value, Re$_b$. Hence, hysteresis occurs between Re$_b$ and Re$_c$. As a consequence, the measured points divide into two groups, low and high intensities. The groups form two branches, a high intensity branch (high V values) and a low intensity branch (low V values), that were used to construct the regime diagram in Tasaka and Iima [19]. Table II lists the critical Reynolds numbers of Re$_b$ and Re$_c$ as well as the gap Reynolds number Re$_g$ for disks with different materials and different gap sizes ΔR; the three left columns list data for the present disks whereas the two right columns list data for disks used in previous work, Tasaka *et al.* [18] and Suzuki *et al.* [17]. The width of the hysteresis region, Re$_c -$ Re$_b$, decreases monotonically with ΔR [indicated by three horizontal arrows in Fig. 3(a)]. The detailed characteristics of the branches and corresponding flow states are discussed below.

First, consider the relationship between Re$_c$ and wettability of the disk. Indicated by Re$_c$ (disk (B)) in Fig. 3(a), the Re$_c$ of disk (B) is the smallest (right end of the 2nd arrow from the bottom of the figure) despite the gap width being intermediate among the three gaps here. This is unexpected as one would assume that increasing the gap and the resulting noise would lead to increases in the destabilization of the flow, and that Re$_c$ would decrease as ΔR increases. This result may be ascribed to the disk material, glass for disk (B), which provides better wettability for the test fluid on the disk. Here a fine air column at the disk center was observed, and that could sustain the attachment of the free surface to the disk by surface tension as suggested in Fig. 3(c). The critical Reynolds number Re$_b$ at the left end of the hysteresis region decreases monotonically with decreasing ΔR as wettability of the test fluid has not influence over the disk at Re$_c$.

Second, consider the relationship between the gap and

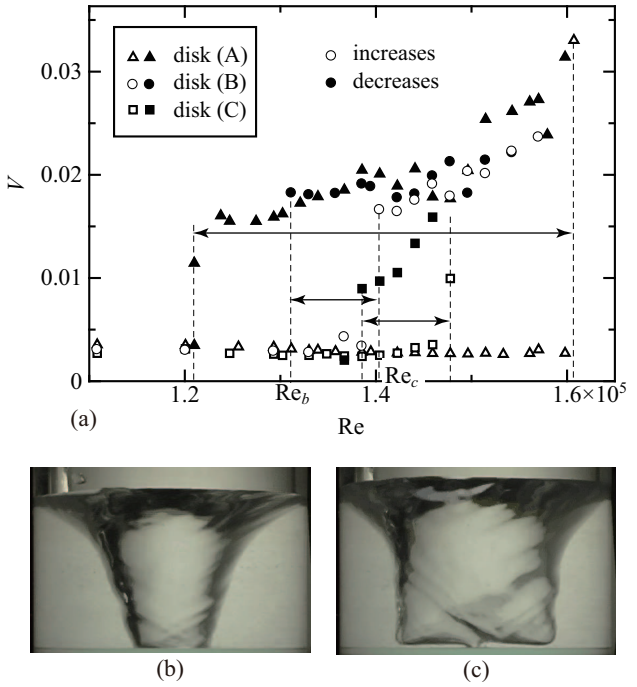

FIG. 3. (a) Variation of the intensity of the velocity fluctuations, V, vs Re, where the open and solid symbols represent the increasing and decreasing stages, respectively, of Re: arrows indicate the range of the hysteresis region for the disks. (b) Photograph of the surface shape for disk (B) at $\mathrm{Re} = 1.11 \times 10^5$ ($\Omega = 10.0$ Hz) and (c) at $\mathrm{Re} = 1.40 \times 10^5$ ($\Omega = 12.7$ Hz).

the boundary of the flow regime. Figure 3(a) shows that V assumes similar values for all disks on the low intensity branch and for values of V for disks (A) and (B) in the region $\mathrm{Re} < \mathrm{Re}_c$ (disk (B)) on the high intensity branch. In both cases, a single flow state is dominant—i.e., the laminar state for the low intensity branch and FR for the high intensity branch.

In contrast, in some regions of the flow regimes, V assumes different values. The high intensity branch (high V values) for disk (C) [Fig. 3(a)] is very different from the other two high intensity branches for disks (A) and (B). The figure shows that V clearly decreases with decreasing Re in the high intensity branch for $\mathrm{Re} < \mathrm{Re}_c$ (disk (C)). In this hysteresis region, there are frequent LTS events and V assumes relatively smaller values than for the other two disks where the free surface maintains RO or FR states, and LTS events are rare.

V. STATISTICAL ANALYSIS OF SURFACE SWITCHING

Controlling the rate of appearance of LTS events by using the disk-rim gap allows a statistical analysis of the LTS events to be performed; in particular, the statistical aspects of the appearance of LTS events can be analyzed. We used two time series of $\langle h(t)\rangle$, each around 650 s long, for a total 1,300 s including the time series shown in Fig. 2(c). To determine an empirical criterion for an LTS event, the $h(t)$ and instantaneous surface shape captured in video clips were compared. The observations showed that the LTS events accompanying the restoration of the axisymmetric shape on the free surface occurs at $\langle h\rangle/H < 0.20$, and the empirical criterion to distinguish LTS events from the time series of $\langle h\rangle$ as $\langle h\rangle/H < 0.20$ was used. Next, the time interval between two successive LTS events, t_s, was defined as the interval between the minima of $\langle h(t)\rangle$ satisfying $\langle h\rangle/H < 0.20$, indicated in Fig. 2(c), where the free surface is attached to the bottom for some duration. The time of attachment and detachment are used to determine t_s [cf. Fig. 2(c)]. In the series, we observed 67 LTS events and the maximum and the minimum durations of t_s were 148.52 s and 7.10 s. To investigate the randomness of the series of t_s, we calculated the auto-correlation defined by

$$C_{t_s}[j] = \frac{\sum_{i=1}^{N} t_s'[i] t_s'[i+j]}{\sum_{i=1}^{N} t_s'[i]^2}, \tag{1}$$

where $t_s'[i]$ is the deviation of the i-th element against the average of $\{t_s[i] \mid i = 1, 2, \cdots, N\}$, and N is the total number of LTS events in a single 650 s long series, $N = 30$. As shown in Fig. 4, the auto-correlation assumes small values throughout, except at the zero time delay at $j = 0$, allowing the conclusion that the t_s series has no periodicity or regularity.

The statistical aspects for the t_s were analyzed as follows. For the probability density function of t_s, $p(t_s)$, [Fig. 5], the nested figure shows the cumulative distribution of $p(t_s)$ calculated from

$$P(\tau_1) = \int_{\tau_1}^{\infty} p(t_s) dt_s, \tag{2}$$

TABLE II. Critical Reynolds numbers at the surface switching, Re_c and Re_b, and the Reynolds number for gap flows corresponding to Re_c and Re_g, for various disks used, specifically, those of the present study and of previous work

	Present disks			In previous work	
	disk (A)	disk (B)	disk (C)		
ΔR [mm]	0.10	0.30[*1]	1.05	0.30[*2]	0.5[*3]
Material	Acrylic	Glass	Acrylic	Acrylic	Glass
$\mathrm{Re}_c(\times 10^5)$	1.61	1.40	1.48	1.55	1.31[*4]
$\mathrm{Re}_b(\times 10^5)$	1.21	1.29	1.37	1.45	
$\mathrm{Re}_g(\times 10^3)$	0.38	1.00	3.70	1.11	1.56

[*1] also used in Tasaka and Iima [19]
[*2] sharp edge at the rim Tasaka *et al.* [18]
[*3] no fixed axis of rotation: ΔR changes from time to time and the value indicated here represents the mean value of ΔR [17]
[*4] hysteresis is not observed and there are no distinctly different values of Re_c and Re_b

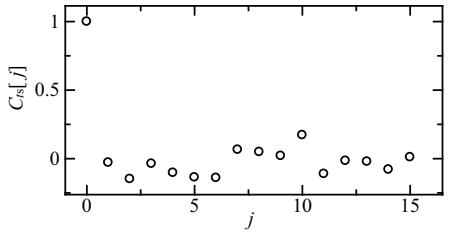

FIG. 4. Auto-correlation function of the series of time intervals for LTS event, $\{t_s[i]\}$

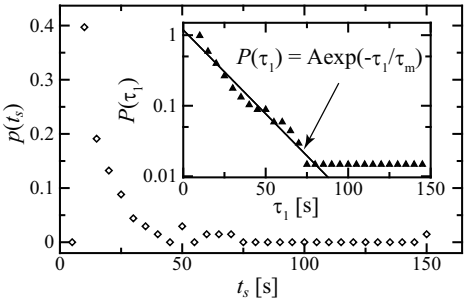

FIG. 5. Probability density distribution of the time interval for the appearance of LTS events, t_s, where the panel inside the larger panel expresses the cumulative distribution of t_s, eq. (5.3).

and this distribution is well approximated by

$$P(\tau_1) = A \exp\left(-\tau_1/\tau_m\right). \tag{3}$$

This indicates the probability of t_s, for $t_s < 75$ s obeying a Poisson distribution, and from this a characteristic time scale for t_s, τ_m, of 18.25 s is obtained.

These results suggest that LTS events are memory-less random events [e.g. 28, 29], and suggest that internal noise may trigger a LTS event. The origin of the internal noise may be assumed to be random noise generated at the disk-rim gap as expected in § II B, even though the mechanism of generation, including the transfer and amplification of the noise in causing the LTS events, are still not determined. Other possibilities of a source of the internal noise generation are edge flow and impact of the radial flow to the lateral wall, also interaction of them including the gap flow. Especially, the edge flow nearby the disk rim has importance to introduce boundary layer transitions on a rotating disk in cases without the lateral wall [30, 31]. The side wall and the top free surface of the present closed system make the behavior of the boundary layer transition much more complicated, because of expectation of stronger radial flows on the disk, corner flows and interactions with Stewartson layer on the side wall. Existence of a cavity below the disk also has possibility to amplify or damp the created noise (even conditions in this study). The present UVP measurement, however, cannot distinguish each source, because of relatively large measurement volume and radial flow measurement. More detailed measurements around the disk rim including the disk-rim gap, for example, boundary layer measurement using laser Doppler anemometer designed for precise measurement in the present system, are required to determine the source.

VI. DIRECT NOISE INJECTION

This section examines the effect of directly injected noise on surface-switching phenomenon as external noise in addition to the internal noise generated in the disk-rim gap. To disturb the flow a small hexa-key (around 5 mm in the mean diameter) was temporarily inserted near the cylinder wall close to the bottom disk, and the velocity fluctuation was measured from UVP to determine the influence of the direct noise on the following transitions. Disk (A) was selected for maintaining a low internal noise condition. The setting Reynolds number is $\mathrm{Re} = 1.48 \times 10^5$ ($\Omega = 13.3$ Hz), in the hysteresis region, and the flow was initially disturbed so that the free surface has a nonaxisymmetric shape.

Figure 6 shows the time variations of the r.m.s. values of the spatial velocity fluctuation measured from UVP to represent the intensity of the spatial velocity fluctuations [see Ref. 19]. The horizontal arrows indicate the duration of disturbing flows arising from the hexa-key; we examined the effect of both (A) a longer duration and (B) a shorter duration disturbance.

For the longer duration disturbance, around 4 s, the pressure balance of the flow is modified by weak mixing caused by inserting the key; the flow does not maintain its nonaxisymmetric free surface with humps (i.e., transition occurs). Following this, the free surface restores the original axisymmetric shape and continues the descent toward the bottom disk also after removing the hexa-key. Despite the axisymmetric state being potentially stable because the system is in the hysteresis region, an LTS (laminar → turbulent) occurs following reattachment to the disk; i.e., the free surface detaches from the disk at the time indicated by the left vertical arrow in the figure.

For the shorter duration disturbance, shorter than 1 s, the flow initially increases in intensity, before an LTS (turbulent → laminar) occurs and the free surface reattaches to the bottom similar to the LTS events caused by internal noise [Fig. 2]. Also here the free surface first restores the original axisymmetric shape, and hence the LTS (laminar → turbulent) occurs accompanied by a nonaxisymmetric free surface with elliptical cross-section. Bergmann *et al.* [11] performed a similar experiment in a shallower fluid layer using a larger cylinder and observed several different rotating polygons. In Bergmann *et al.* [11], the disturbed flow restores initially the axisymmetric shape, then elliptic, triangular, and other polygonal shapes with a larger number of vertices occur in the time series. Our results show similar behavior, however, here it must be noted that after the free surface reattaches to the bottom with both long- and short-duration-added disturbances, the free surface detaches from the bottom

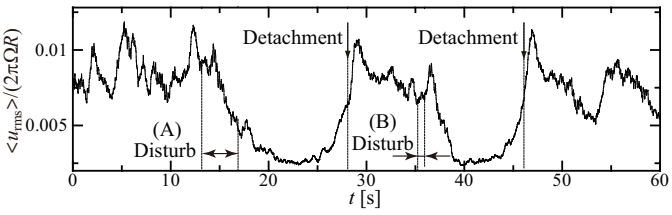

FIG. 6. Time variation of r.m.s. values of the spatial velocity fluctuation disturbing the flow by inserting a small hexa-key (around 5 mm in mean diameter) in the vessel: horizontal arrows indicate the duration of disturbances, (A) a longer duration and (B) a shorter duration: vertical arrows indicate time of detachment of the free surface from the bottom

and the corresponding r.m.s. values of the velocity fluctuation increase in a very similar progression. Specifically, the particular flow structure generated during the LTS (laminar → turbulent) events expires rather quickly. This supports the suggestion that the LTS (turbulent → laminar) is memory-less as explained in §V, and in particular shown by Fig. 5.

VII. DISCUSSION

A. Disk-rim gap and internal noise

As introduced in § II B, the flow in the disk-rim gap at the cylinder wall can be a chaotic or turbulent flow, generating internal noise in the bulk flow. There is evidence that a small change in the disk-rim gap changes some of the characteristics in the rotating flow. For closed flows with a rotating disk in a cylindrical vessel, a model system for subcritical-flow instability problems in Couette flows, Le Gal *et al.* [24] investigated the effect of the disk-rim gap and established that the appearance of local turbulence at the disk rim was clearly dependent on the size of the disk-rim gap, suggesting the possibility of controlling the internal noise by modifying the disk-rim gap.

In a more general sense, the internal noise can trigger irregular transitions of large-scale fluid motions. Experimentally, in subcritical-flow instability problems in wall-bounded turbulence [32, 33], the addition of finite-amplitude perturbations triggers local turbulence and relaminarization occurs via a stochastic process. In other systems such as irregular flow reversals of large-scale circulation in natural convections [29, 34, 35] and reversals of flow between counter-rotating disks (von Kármán swirling flow) [36, 37], noise originates from internal small-scale turbulent motions, and mathematical models have been proposed to describe the phenomena by considering internal noise as a stochastic term [e.g. 35, 37, 38].

Lastly, we remark on the uncertainty in the critical Reynolds number in a system with internal noise. In our experiments, there would be a lowest limiting Re to sustain the high intensity branch in an ideal environment without gap noise. Nevertheless, in actual situations, the condition associated with the high intensity branch expires at a larger Re because of the influence of internal noise: Internal noise generated at the disk-rim gap supports a flow state to exceed the basin boundary (boundary of quasi-stable states in state space) between the branches. Also, such effect of the internal noise partially account for the reason that the range of the hysteresis region depends on the strength of the internal noise. This is why Re_b and range of the hysteresis region shown in Fig. 3 depend on ΔR.

B. Effect of internal noise on the surface switching dynamics

Sato *et al.* [39] provided a simple mathematical model that included a stochastic term to describe internal noise for the surface switching phenomena. It was based on measurement data of the free surface height fluctuations at the center of the cylinder and the intensity of the spatial velocity fluctuations [19]. The model is a one-dimensional return map describing the minimum and maximum positions of the surface height fluctuations with noise term, which was assumed to have a Gaussian distribution where the magnitude is a function of the surface height. In this section, we interpret the results based on this model.

Parametric studies of the model have indicated that modifying the noise term can reproduce the typical results observed in both Suzuki *et al.* [17] and Tasaka and Iima [19]. Overall, the results of this model suggest that an increase in internal noise increases the frequency of appearance of the surface descending events.

In this model, there are two equilibria or balancing points in instances without noise, corresponding to the FR state ($h > 0$, stable) and the TA state ($h = 0$, unstable). We discuss the effect of the noise term in detail below. To help the discussion, we show a schematic view (Fig. 7) of the balancing points and relate events at each noise level. The vertical and horizontal extents indicating degree of surface height and velocity fluctuation, respectively, form a state space, where the color for each closed area represents the stability or duration of each state, specifically, white, low, and very short; gray, moderate; and black, high and long. The arrows display the available transition between the states.

In the model of Sato *et al.* [39], the FR is a relatively frequent quasi-steady state under lower noise conditions that occasionally fluctuates because of noise and may correspond to narrow rim-gap situations in actual experiments [see Figs. 2(a) and 7(a)].

This quasi-steady state becomes unstable when affected by moderate internal noise, and a transition to the RO state occurs. Corresponding to this condition in the experiments, there is a moderate rim-gap [see Figs. 2(b) and 7(b)]. The RO is a quasi-periodic oscillatory state that arises by a different "dynamic balance" (as a quasi-

periodic state) from that at FR.

The FR state becomes invisible under high noise conditions, and may correspond to large rim-gap situations in actual experiments [see Figs. 2(c) and 7(c)]. The differences between the states in the model arising from different noise levels are similar to that between the rates of appearance of the RO state and the FR state in different disk-rim gap conditions.

Parametric studies on the mathematical model by Sato *et al.* [39] provided helpful suggestions to understand the detail of the transition of the regime, especially the formation of the hysteresis region shown in Fig. 3. In their model, two balancing points corresponding to the high and the low intensity blanches in the regime diagram, are assumed, and the regions between the balancing points are bounded by the basin boundary, which depends on stability of the points. Increasing the noise level induces transition beyond the boundary, and thus the hysteresis region becomes narrower. Further, a much larger noise would remove the hysteresis region observed in Suzuki *et al.* [17].

VIII. CONCLUSION

We examined the influence of internal noise on surface switching phenomena accompanying transitions between turbulent and laminar flows in a rotating fluid with a free surface. To modify the internal noise we used three disks of different sizes, each giving a different disk-rim spacing at the cylinder wall. The influence of the gaps was investigated dynamically and statistically from data of the radial velocity and free surface height fluctuations at the center of the cylinder. The results suggest that surface switching accompanying the transition from turbulent flow to laminar flow, termed LTS (turbulent $\rightarrow$ laminar), is triggered by the gap noise and is a random, memory-less event. The gap noise also induces transitions between two different quasi-stable states, FR characterized by very small fluctuations of the surface height and RO characterized by larger, quasi-periodic fluctuations of the surface height, and that situations with high internal noise produce a diffuse boundary between FR and RO. Regime diagrams obtained with each disk showed that a large gap noise narrows the hysteresis region that is characteristic of the high and low intensity branches of the velocity fluctuations. These results closely agree with the predictions from a simple mathematical model of the surface switching phenomena that incorporates a noise term with a one-dimensional return map [39].

ACKNOWLEDGMENT

The idea to control internal noise adopted in this study arose in fruitful discussions with Professor Yuzuru Sato, and described in his corresponding paper, for which the authors are gratefully thankful. This study was supported by Core Research for Evolutional Science and Technology (CREST) No. PJ74100011 and Grants-in-Aid for Scientific Research (25420103).

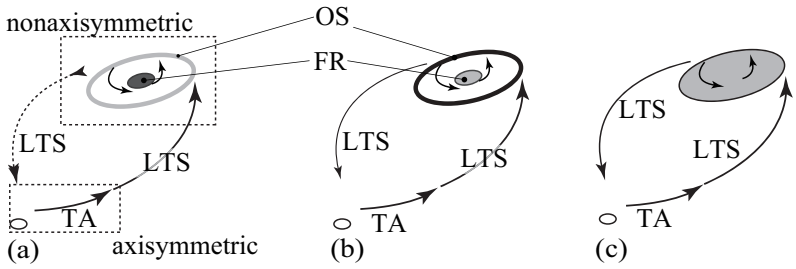

FIG. 7. Schematic view of the balancing points embedded in the phenomena and relating events for (a) low, (b) moderate, and (c) high noise conditions, where vertical and horizontal extents indicate the degree of surface height and velocity fluctuation; color of an area represents stability or sojourn time of each state: white—low and very short, gray—moderate, and black—high and long

[1] E. R. Benton and A. J. Clark, Ann. Rev. Fluid Mech. **6**, 257 (1974).
[2] H. P. Greenspan, in *The theory of rotating fluids* (Cambridge, 1968).
[3] M. P. Escudier, Exp. Fluids **2**, 189 (1984).
[4] J. Lopez, F. Marques, A. H. Hirsa, and R. Miraghaie, J. Fluid Mech. **502**, 99 (2004).
[5] S. Fujimoto and Y. Takeda, Phys. Rev. E **80**, 015304(R) (2009).
[6] P. T. Brady, M. Herrmann, and J. M. Lopez, Phys. Rev. E **85**, 016308 (2012).
[7] L. Kahouadji and L. M. Witkowski, Phys. Fluids **26**, 072105 (2014).
[8] G. H. Vatistas, J. Fluid Mech. **217**, 241 (1990).
[9] T. R. N. Jansson, M. P. Haspang, K. H. Jensen, P. Hersen, and T. Bohr, Phys. Rev. Lett. **96**, 174502 (2006).
[10] G. H. Vatistas, H. A. Abderrahmane, and M. H. K. Siddiqui, Phys. Rev. Lett. **100**, 174503 (2008).
[11] R. Bergmann, L. T. j, T. A. M. Homan, P. Hensen, A. Andersen, and T. Bohr, J. Fluid Mech. **679**, 411 (2011).
[12] H. A. Abderrahmane, K. Siddiqui, G. H. Vatistas, M. Fayed, and H. D. Ng, Phys. Rev. E **83**, 056319 (2011).
[13] L. Tophoj, J. Mougel, T. Bohr, and D. Fabre, Phys. Rev. Lett. **110**, 194502 (2013).
[14] K. Iga, S. Yokota, S. Watanabe, T. Ikeda, H. Niino, and N. Misawa, Fluid Dyn. Res. **46**, 031409 (2014).
[15] D. Fabre and J. Mougel, Fluid Dyn. Res. **46**, 061415 (2014).
[16] B. Bach, E. C. Linnartza, M. H. Vesteda, A. Andersena, and T. Bohr, J. Fluid Mech. **759**, 386 (2014).
[17] T. Suzuki, M. Iima, and Y. Hayase, Phys. Fluids **18**, 101701 (2006).
[18] Y. Tasaka, M. Iima, and K. Ito, J. Phys.: Conference Series **137**, 012030 (2008).
[19] Y. Tasaka and M. Iima, J. Fluid Mech. **636**, 475 (2009).
[20] M. Iima and Y. Tasaka, J. Fluid Mech. **789**, 402 (2016).
[21] J. M. D. Fabre and L. Lacaze, Machanics & Industry **15**, 107 (2014).
[22] Y. Takeda, JSME Intl. J. **B38**, 8 (1995).
[23] in *Ultrasonic Doppler velocity profiler for fluid flow*, Vol. 101, edited by Y. Takeda (Springer, 2012).
[24] P. Le Gal, Y. Tasaka, J. Nagao, A. Cros, and K. Yamaguchi, J. Engng. Math. **57**, 289 (2007).
[25] T. Watanabe and H. Furukawa, Exp. Fluids **48**, 631 (2010).
[26] C. D. Andereck, S. S. Liu, and H. L. Swinney, J. Fluid Mech. **164**, 155 (1986).
[27] H. L. Reed and W. S. Saric, Ann. Rev. Fluid Mech. **21**, 235 (1989).
[28] B. Hof, J. Westerweel, T. M. Schneider, and B. Eckhardt, Nature **443**, 59 (2006).
[29] K. R. Sreenivasan, A. Bershadskii, and J. J. Niemela, Phys. Rev. E **65**, 056306 (2002).
[30] S. Imayama, P. H. Alfredsson, and R. J. Lingwood, J. Fluid Mech. **716**, 638 (2013).
[31] B. Pier, J. Fluid Mech. **737**, R1 (2013).
[32] T. Mullin, Ann. Rev. Fluid Mech. , 14 (2010).
[33] P. Manneville, J. Mech. B Fluids **49**, 345 (2015).
[34] K. Sugiyama, R. Ni, R. J. A. M. Stevens, T. S. Chan, S.-Q. Zhou, H.-D. Xi, C. Sun, S. Grossmann, K.-Q. Xia, and D. Lohse, Phys. Rev. Lett. **105**, 034503 (2010).
[35] R. Ni, S.-D. Hung, and K.-Q. Xia, J. Fluid Mech. **778**, R5 (2015).
[36] F. Ravelet, L. Marie, A. Chiffaudel, and F. Daviaud, Phys. Rev. Lett. **93**, 164501 (2004).
[37] A. de la Torre and J. Burguete, Phys. Rev. Lett. **99**, 054101 (2007).
[38] D. Barkley, Phys. Rev. E **84**, 016309 (2011).
[39] Y. Sato, M. Iima, and Y. Tasaka, Hokkaido University Preprint Series in Mathematics , No. 979 (2011).